

Title	Flow-induced scission of wormlike micelles in nonionic surfactant solutions under shear flow
Author(s)	Koide, Yusuke; Goto, Susumu
Citation	Journal of Chemical Physics. 2022, 157(8), p. 084903
Version Type	VoR
URL	https://hdl.handle.net/11094/90766
rights	This article may be downloaded for personal use only. Any other use requires prior permission of the author and AIP Publishing. This article appeared in Koide Y., Goto S. Flow-induced scission of wormlike micelles in nonionic surfactant solutions under shear flow. Journal of Chemical Physics 157, 084903 (2022) and may be found at https://doi.org/10.1063/5.0096830 .
Note	

Osaka University Knowledge Archive : OUKA

<https://ir.library.osaka-u.ac.jp/>

Osaka University

Flow-induced scission of wormlike micelles in nonionic surfactant solutions under shear flow

Cite as: J. Chem. Phys. **157**, 084903 (2022); <https://doi.org/10.1063/5.0096830>

Submitted: 22 April 2022 • Accepted: 21 July 2022 • Accepted Manuscript Online: 25 July 2022 •

Published Online: 30 August 2022

 Yusuke Koide and  Susumu Goto



View Online



Export Citation



CrossMark

ARTICLES YOU MAY BE INTERESTED IN

[Computation of NMR shieldings at the CASSCF level using gauge-including atomic orbitals and Cholesky decomposition](#)

The Journal of Chemical Physics **157**, 084122 (2022); <https://doi.org/10.1063/5.0101838>

[Deep learning-based quasi-continuum theory for structure of confined fluids](#)

The Journal of Chemical Physics **157**, 084121 (2022); <https://doi.org/10.1063/5.0096481>

[Gaussian product rule for two-electron wave functions](#)

The Journal of Chemical Physics **157**, 084123 (2022); <https://doi.org/10.1063/5.0101387>



Time to get excited.
Lock-in Amplifiers – from DC to 8.5 GHz

Find out more

Zurich Instruments

Flow-induced scission of wormlike micelles in nonionic surfactant solutions under shear flow

Cite as: *J. Chem. Phys.* **157**, 084903 (2022); doi: [10.1063/5.0096830](https://doi.org/10.1063/5.0096830)

Submitted: 22 April 2022 • Accepted: 21 July 2022 •

Published Online: 30 August 2022



View Online



Export Citation



CrossMark

Yusuke Koide^{a)}  and Susumu Goto^{b)} 

AFFILIATIONS

Graduate School of Engineering Science, Osaka University, 1-3 Machikaneyama, Toyonaka, Osaka 560-8531, Japan

^{a)} Author to whom correspondence should be addressed: y_koide@fm.me.es.osaka-u.ac.jp

^{b)} Electronic mail: s.goto.es@osaka-u.ac.jp

ABSTRACT

We investigate flow-induced scission of wormlike micelles with dissipative particle dynamics simulations of nonionic surfactant solutions under shear flow. To understand flow-induced scission in terms of micellar timescales, we propose a method to evaluate the longest relaxation time of unentangled surfactant micelles from the rotational relaxation time and the average lifetime at equilibrium. The mean squared displacement of surfactant molecules provides evidence that the longest relaxation time estimated by the proposed method serves as the characteristic timescale at equilibrium. We also demonstrate that the longest relaxation time plays an essential role in flow-induced scission. Using conditional statistics based on the aggregation number of micelles, we examine the statistical properties of the lifetime of wormlike micelles. We then conclude that flow-induced scission occurs when the Weissenberg number defined as the product of the longest relaxation time and the shear rate is larger than a threshold value.

Published under an exclusive license by AIP Publishing. <https://doi.org/10.1063/5.0096830>

I. INTRODUCTION

Surfactants consist of hydrophilic and hydrophobic moieties. Above a critical concentration, surfactants spontaneously assemble into aggregates such as spherical micelles, rodlike micelles, and wormlike micelles in aqueous solutions.¹ Since these micelles exhibit unique properties, they can serve as additives in working fluids for various applications, including rheology control,² turbulent drag reduction,³ and drug delivery systems.⁴ Therefore, it is crucial to understand the structures and dynamics of micelles in flowing solutions for industrial applications of surfactants.

Flow-induced scission of surfactant micelles is among the crucial phenomena. Although thermal fluctuations induce scission of micelles at equilibrium, flow with high velocity gradients promotes their scission.^{5–7} This phenomenon may be intuitively obvious, but it is difficult to quantitatively predict the conditions and degree of flow-induced scission, which are required for practical use of surfactants. An increase in scission frequency brings about a drastic change in micellar structures and distributions, leading to a significant modification of the flow properties of surfactant solutions.^{8,9–10} In addition, since the constitutive equations for surfactant solutions need to include the effect of scission and recombination kinetics explicitly,^{11–13} insight into flow-induced micellar scission leads

to an understanding of the rheology and turbulent drag reduction phenomenon of surfactant solutions. In other words, to reveal the macroscopic flow behavior of surfactant solutions, we need to understand the properties of flow-induced micellar scission. In the present study, we focus on a uniform shear flow, which is often used in rheological measurements, and investigate flow-induced scission of wormlike surfactant micelles in detail.

Although some experimental studies succeeded in evaluating the average lifetime of micelles,^{14–16} it is difficult to experimentally observe the structures and dynamics of individual micelles in flowing solutions. Molecular simulations allow us to overcome this difficulty with measurements. When we are interested in the slow dynamics of micelles rather than the fast dynamics at the atomic level, coarse-graining, in which several atoms or molecules are considered as a single particle, is often used to reduce the computational cost associated with all-atom molecular dynamics simulations. The coarse-grained molecular dynamics (CGMD) method using the MARTINI force field is one of the most popular approaches based on coarse-graining. With CGMD, we can simulate micellar scission to evaluate relevant micellar properties directly.^{17,18} Regarding flow-induced scission, Sambasivam *et al.*¹⁹ conducted CGMD simulations of a single rodlike micelle under shear flow and found that elongation of micelles by a shear flow increased the potential energy,

thus leading to the scission of micelles. Although CGMD simulations have revealed the detailed dynamics of micellar scission, many studies simulated a single micelle or a few micelles only.^{17–19} Therefore, the statistical properties of flow-induced scission and its effect on the micellar distribution remain unclear.

Another coarse-graining approach relies on the introduction of a kinetic model for scission and recombination, and several models^{20–22} have been proposed. These models significantly reduce the computational cost and allow systematic investigation of the statistical properties of scission and recombination. Kröger and Makhlofi²⁰ proposed the FENE-C model, which introduces scission and recombination into a finitely extensible nonlinear elastic (FENE) potential. They reported the shear-rate dependence of the average micellar length and lifetime under shear flow. Padding *et al.*²² modeled a wormlike micelle as a string of thin rods and found that the average breaking rate varied depending on the scission energy and shear rate $\dot{\gamma}$. However, there is still room for consideration of these results concerning flow-induced scission because scission and recombination were explicitly modeled in these previous studies. Moreover, the explanation of the shear-rate dependence of flow-induced scission was unsatisfactory because relevant timescales of individual micelles were not considered.

It is well known that the relaxation time of micelles, which repeatedly break and recombine, is sometimes affected by scission. Regarding entangled micelles, Cates²³ proposed a theory that predicts the relaxation time from the average lifetime and reptation time of micelles. On the other hand, for unentangled micelles, Faivre and Gardissat²⁴ proposed a theory that incorporated the process of scission and recombination into the Rouse model, although they aimed at describing the viscoelasticity of amorphous selenium. Huang *et al.*²⁵ numerically confirmed the validity of this theory. According to the concept proposed by Faivre and Gardissat, Huang *et al.* defined the relaxation time τ_Λ of micelles, which corresponds to the relaxation time of a segment of size Λ for which the lifetime is equal to the Rouse relaxation time. They found that chain deformation, orientation, and rheological properties under shear flow are expressed by universal functions of the dimensionless number $\beta_\Lambda = \tau_\Lambda \dot{\gamma}$. However, their simulations used a mesoscopic model incorporating a kinetic model for scission and recombination into linear chains. To our knowledge, no study has examined whether τ_Λ also plays a crucial role in unentangled micelles composed of surfactant molecules. Since surfactant micelles have complicated internal structures compared with polymer-like linear chains, they exhibit complex dynamics of scission and recombination. Therefore, the applicability of τ_Λ to surfactant micelles is not obvious and is worth studying.

In the present study, we intend to quantitatively reveal the shear-rate dependence of micellar scission and identify the timescales relevant to flow-induced scission. For this purpose, we conduct molecular simulations of nonionic surfactant solutions using the dissipative particle dynamics (DPD) method. DPD was proposed by Hoogerbrugge and Koelman²⁶ and then improved by Español and Warren.²⁷ Many researchers^{28–34} have extensively investigated surfactant solutions using the DPD method. Since particles interact via soft repulsive interactions in DPD, we can make time steps larger than CGMD, which allows us to simulate large systems for long timescales with a low computational cost. Therefore, we can evaluate the statistical properties of flow-induced scission and

its effect on the micellar distribution. Since previous studies^{20,22,25} have analyzed the average properties over all the micelles in the system, their results could demonstrate only the combined effect of the changes in micellar properties and distributions. We overcome this problem using conditional statistics based on the aggregation number of micelles, which offer deeper insight into the shear flow effect on individual micelles. In addition, we introduce the longest relaxation time of unentangled micelles to demonstrate that a single dimensionless number can characterize flow-induced scission. More concretely, we extend the theory of Faivre and Gardissat²⁴ to unentangled surfactant micelles. We then prove the importance of this timescale in micellar scission under shear flow using the simulation results for various temperatures.

II. SIMULATION METHOD

A. DPD governing equations

In DPD simulations, we regard a group of atoms and molecules as a single DPD particle. The motion of a DPD particle obeys

$$m_i \frac{d\mathbf{v}_i}{dt} = \sum_{j(\neq i)} \mathbf{F}_{ij}^C + \sum_{j(\neq i)} \mathbf{F}_{ij}^D + \sum_{j(\neq i)} \mathbf{F}_{ij}^R, \quad (1)$$

where m_i and \mathbf{v}_i are the mass and velocity of the i th particle, respectively, and \mathbf{F}_{ij}^C , \mathbf{F}_{ij}^D , and \mathbf{F}_{ij}^R are the conservative, dissipative, and random forces exerted on the i th particle by the j th particle, respectively. The conservative force acts as a repulsive force in the form of

$$\mathbf{F}_{ij}^C = \begin{cases} a_{ij} \left(1 - \frac{r_{ij}}{r_c}\right) \mathbf{e}_{ij} & \text{for } r_{ij} \leq r_c, \\ 0 & \text{for } r_{ij} > r_c, \end{cases} \quad (2)$$

where a_{ij} is the conservative force coefficient between the i th and j th particles, r_c is the cutoff distance, $\mathbf{r}_{ij} = \mathbf{r}_i - \mathbf{r}_j$, $r_{ij} = |\mathbf{r}_{ij}|$, and $\mathbf{e}_{ij} = \mathbf{r}_{ij}/r_{ij}$ with \mathbf{r}_i being the position of the i th particle. The dissipative and random forces are expressed as

$$\mathbf{F}_{ij}^D = -\gamma w^D(r_{ij}) (\mathbf{e}_{ij} \cdot \mathbf{v}_{ij}) \mathbf{e}_{ij} \quad (\mathbf{v}_{ij} = \mathbf{v}_i - \mathbf{v}_j) \quad (3)$$

and

$$\mathbf{F}_{ij}^R = \sigma w^R(r_{ij}) \theta_{ij} \mathbf{e}_{ij}, \quad (4)$$

where γ and σ are the dissipative and random force coefficients, respectively, and $w^D(r_{ij})$ and $w^R(r_{ij})$ are the weight functions of the dissipative and random forces, respectively. In Eq. (4), θ_{ij} is a random variable that satisfies

$$\begin{cases} \theta_{ij}(t) = \theta_{ji}(t), & (5) \\ \langle \theta_{ij}(t) \rangle = 0, & (6) \\ \langle \theta_{ij}(t) \theta_{kl}(t') \rangle = (\delta_{ik} \delta_{jl} + \delta_{il} \delta_{jk}) \delta(t - t'), & (7) \end{cases}$$

where δ_{ij} is the Kronecker delta, $\delta(t)$ is the delta function, and $\langle \cdot \rangle$ denotes the ensemble average. The fluctuation dissipation theorem requires that γ , σ , $w^D(r_{ij})$, and $w^R(r_{ij})$ satisfy

$$w^D(r_{ij}) = [w^R(r_{ij})]^2 \quad (8)$$

and

$$\sigma^2 = 2\gamma k_B T, \quad (9)$$

where k_B is the Boltzmann constant and T is the temperature of the system.²⁷ Following Ref. 35, we set the weight function $w^R(r_{ij})$ as

$$w^R(r_{ij}) = \begin{cases} 1 - \frac{r_{ij}}{r_c} & \text{for } r_{ij} \leq r_c, \\ 0 & \text{for } r_{ij} > r_c. \end{cases} \quad (10)$$

In what follows, we use simulation units with $k_B T_0 = m = r_c = 1$, where T_0 is the reference temperature.

B. Surfactant model

The system is composed of water and nonionic surfactants. Since we focus on the general properties of flow-induced scission, we do not assume any specific species of surfactant molecule in the following. As shown in Fig. 1, a surfactant molecule contains a hydrophilic particle and two hydrophobic particles, which are connected by harmonic springs expressed by

$$\mathbf{F}_{ij}^B = -k_s(r_{ij} - r_{eq})\mathbf{e}_{ij}, \quad (11)$$

where k_s is the spring constant and r_{eq} is the equilibrium bond distance. We show the simulation parameters in Table I. Here, N is the total number of DPD particles, ρ is the number density of DPD particles, ϕ is the volume fraction of surfactants, and a_{ij} is the conservative force coefficient between different types of particles. The subscripts indicate the types of particles: h, t, and w denote the head, tail, and water particles, respectively. Here, we determine a_{ij} according to Ref. 36 because wormlike micelles are found to be formed for this model above a certain volume fraction. We choose $\phi = 0.05$ for a sufficient number of wormlike micelles to exist in the system. For a specific species of surfactant molecule, a_{ij} can be obtained using a parameterization scheme.^{35,37–39} When we vary $k_B T$, γ changes so that it satisfies Eq. (9) while fixing the value of σ at 3.

TABLE I. DPD simulation parameters. N is the total number of DPD particles, ρ is the number density of DPD particles, σ is the random force coefficient, ϕ is the volume fraction of surfactants, k_s is the spring constant, r_{eq} is the equilibrium bond distance, and a_{ij} is the conservative force coefficient between different types of particles. The subscripts indicate the types of particles: h, t, and w denote head, tail, and water particles, respectively.

N	ρ	σ	ϕ	k_s	r_{eq}	a_{hh}	a_{ht}	a_{hw}	a_{tt}	a_{tw}	a_{ww}
648 000	3	3	0.05	50	0.8	25	60	20	25	60	25

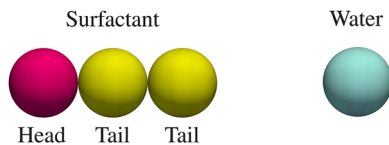


FIG. 1. Schematic of the coarse-grained model of a surfactant and water. The head of the former is a hydrophilic particle, and the tails are hydrophobic particles.

C. Simulation details

To integrate the equations of motion, we use the modified velocity Verlet method,³⁵

$$\begin{aligned} \mathbf{r}_i(t + \Delta t) &= \mathbf{r}_i(t) + \Delta t \mathbf{v}_i(t) + \frac{1}{2}(\Delta t)^2 \mathbf{F}_i(t), \\ \tilde{\mathbf{v}}_i(t + \Delta t) &= \mathbf{v}_i(t) + \lambda \Delta t \mathbf{F}_i(t), \\ \mathbf{F}_i(t + \Delta t) &= \mathbf{F}_i(\mathbf{r}(t + \Delta t), \tilde{\mathbf{v}}_i(t + \Delta t)), \\ \mathbf{v}_i(t + \Delta t) &= \mathbf{v}_i(t) + \frac{1}{2} \Delta t (\mathbf{F}_i(t) + \mathbf{F}_i(t + \Delta t)), \end{aligned} \quad (12)$$

where Δt is the time step, \mathbf{F}_i is the force exerted on the i th particle, λ is the parameter introduced in this algorithm, and $\tilde{\mathbf{v}}_i$ is the predicted velocity of the i th particle. The random force defined by Eq. (4) is expressed by

$$\mathbf{F}_{ij}^R = \sigma w_R(r_{ij}) \zeta_{ij} \Delta t^{-1/2} \mathbf{e}_{ij} \quad (13)$$

when we calculate Eq. (12). In Eq. (13), ζ_{ij} is a Gaussian random variable with zero mean and unit variance. According to Ref. 35, we choose $\lambda = 0.65$ and $\Delta t = 0.04$. We have confirmed that these parameters realize sufficiently accurate temperature control.

In the present study, we use the Lees–Edwards boundary condition⁴⁰ and the so-called SLLOD equations⁴¹ to generate a uniform shear flow as shown in Fig. 2. The SLLOD equations read

$$\begin{aligned} \dot{\mathbf{r}}_i &= \mathbf{p}_i/m_i + \mathbf{r}_i \cdot \nabla \mathbf{u}, \\ \dot{\mathbf{p}}_i &= \mathbf{F}_i - \mathbf{p}_i \cdot \nabla \mathbf{u}, \end{aligned} \quad (14)$$

where \mathbf{p}_i is the so-called peculiar momentum and \mathbf{u} is the fluid stream velocity. In the case of a uniform shear flow, we can express $\nabla \mathbf{u}$ as

$$\nabla \mathbf{u} = \begin{pmatrix} 0 & 0 & 0 \\ \dot{\gamma} & 0 & 0 \\ 0 & 0 & 0 \end{pmatrix}, \quad (15)$$

with $\dot{\gamma}$ being the shear rate. We impose a random initial configuration and conduct equilibrium simulations for 20 000 time units,

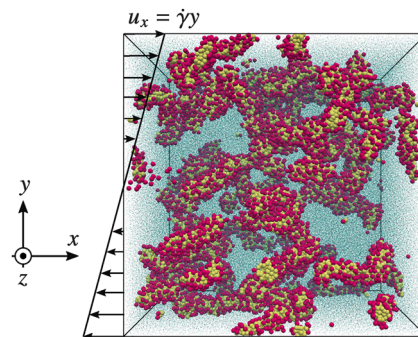


FIG. 2. Visualization of a system composed of surfactants and water. Hydrophilic and hydrophobic particles are indicated in red and yellow, respectively. For clarity, water particles are represented by blue dots.

achieving statistically steady values of the potential energy. After that, we conduct nonequilibrium simulations by imposing shear flow. We perform all the DPD simulations using our in-house code.

We define micelles adopting the method used in previous studies.^{37,42} In this method, we judge that two surfactant molecules belong to a common cluster if a hydrophobic particle of one surfactant molecule is within $r_c (= 1)$ of a hydrophobic particle of the other. If a cluster has an aggregation number N_{ag} larger than a threshold value $n_{mic} (= 10)$, then we regard the cluster as a micelle. Since we focus mainly on micelles with $N_{ag} \gtrsim 50$, our results are practically insensitive to the choice of n_{mic} . When we investigate the N_{ag} dependence of micellar properties, we use conditional statistics based on N_{ag} . More concretely, to evaluate the micellar properties for a given N_{ag} , we use the data for micelles having aggregation numbers that lie in $[N_{ag} - \Delta N_{ag}, N_{ag} + \Delta N_{ag}]$, where we set $\Delta N_{ag} = 0.05N_{ag}$.

III. RESULTS AND DISCUSSION

A. Timescales of micelles

One of the main goals of the present study is to elucidate the shear-rate dependence of flow-induced scission. For this purpose, we first identify the relevant timescales of micelles at equilibrium (i.e., in the absence of shear flow). As will be shown below, the rotational relaxation time τ_r and the average lifetime τ_b of micelles are the keys to understanding the dynamics of unentangled wormlike micelles under shear flow. More concretely, τ_r and τ_b determine their longest relaxation time τ .

The target of the present study is the scission of rodlike and wormlike micelles. As shown in Appendix A, micelles are rodlike when $50 \lesssim N_{ag} \lesssim 200$ and wormlike when $N_{ag} \gtrsim 200$. To estimate τ_r of rodlike and wormlike micelles, we evaluate the rotational autocorrelation function,

$$C(t) = \langle \mathbf{e}^{(1)}(t_0 + t) \cdot \mathbf{e}^{(1)}(t_0) \rangle, \quad (16)$$

where $\mathbf{e}^{(1)}$ is the unit eigenvector of the gyration tensor G_{ij} corresponding to the largest eigenvalue. Here, G_{ij} is defined by

$$G_{ij} = \frac{1}{N_{sur}} \sum_{k=1}^{N_{sur}} \Delta r_{k,i} \Delta r_{k,j}, \quad (17)$$

where $\Delta r_{k,i}$ is the i th component of the relative position vector of the k th surfactant particle with respect to the center of mass of the

micelle and $N_{sur} (= 3N_{ag})$ is the number of surfactant particles in the micelle. Since $-\mathbf{e}^{(1)}$ is also a unit eigenvector of G_{ij} , we determine $\mathbf{e}^{(1)}(t)$ so that $\mathbf{e}^{(1)}(t - \delta t) \cdot \mathbf{e}^{(1)}(t) > 0$, where we set $\delta t = 100\Delta t$. Then we fit $C(t)$ with an exponential function,

$$C(t) = C_0 \exp(-t/\tau_r), \quad (18)$$

where C_0 is a constant, to determine τ_r . Note that we use conditional statistics based on N_{ag} to obtain $C(t)$ for a given N_{ag} . For each micelle, we evaluate $\mathbf{e}^{(1)}(t_0 + t) \cdot \mathbf{e}^{(1)}(t_0)$ until scission, which is defined below, occurs. We show in Fig. 3(a) that $C(t)$ can be expressed well by Eq. (18). Figure 3(b) shows τ_r as a function of N_{ag} . The slope of τ_r for $N_{ag} \gtrsim 200$ is smaller than that for $N_{ag} \lesssim 200$. Since as shown in Appendix A, rodlike micelles change into wormlike micelles above $N_{ag} \simeq 200$, micellar structures affect N_{ag} dependence of τ_r . As shown in Fig. 3(a), it is difficult to obtain $C(t)$ for large N_{ag} with enough accuracy to estimate τ_r . As discussed below, large micelles break into small micelles rapidly, thus making it difficult to acquire data for large t . Therefore, $C(t)$ for $N_{ag} = 400$ is shown within a limited range and fluctuates significantly for large t . As a result, the error bars of τ_r for large N_{ag} are larger than those for small N_{ag} . However, in the case of the parameters used in the present study, the accuracy of τ_r for large N_{ag} has little effect on the determination of the longest relaxation time introduced below.

Next, we investigate the characteristic timescale of micellar scission at equilibrium. Micelles repeatedly break and recombine due to the thermal effect. Here, we focus on the time required for micellar scission and evaluate the average lifetime τ_b of micelles at equilibrium. First, we explain how to detect the scission of micelles. We monitor N_{ag} of each micelle at a certain time interval $\delta t (= 100\Delta t)$, and when a micelle is decomposed into two or more groups, each of which contains more than $n_{mic} (= 10)$ surfactant molecules, we consider that the micelle breaks. Then, we obtain the lifetime t_b of each micelle. By conducting the analysis for different values of n_{mic} in the range $5 \leq n_{mic} \leq 30$, we have confirmed that the choice of n_{mic} has little effect on the following results. To describe the statistics of t_b , we investigate the survival function $S(t_b)$, which gives the probability that micelles survive beyond a certain time t_b . We estimate $S(t_b)$ using the Kaplan–Meier method.⁴³ Figure 4(a) shows $S(t_b)$ for several N_{ag} . We find that $S(t_b)$ obeys an exponential function, which means that micellar scission events occur with a constant probability per unit time. To obtain τ_b , we fit $S(t_b)$ with $C_0 \exp(-t_b/\tau_b)$ except for short times where $S(t_b)$ does not show

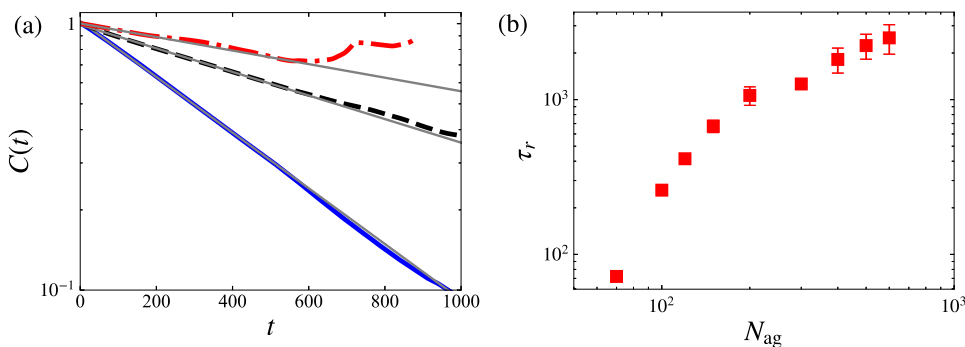


FIG. 3. (a) Rotational autocorrelation function $C(t)$ of micelles for $N_{ag} = 120$ (blue solid line), 200 (black dashed line), and 400 (red dotted-dashed line) at equilibrium with $k_B T = 1$. Gray lines are exponential fits to the data. (b) Rotational relaxation time τ_r of micelles as a function of N_{ag} with $k_B T = 1$. The error bars in (b) denote the standard deviations for three independent simulations.

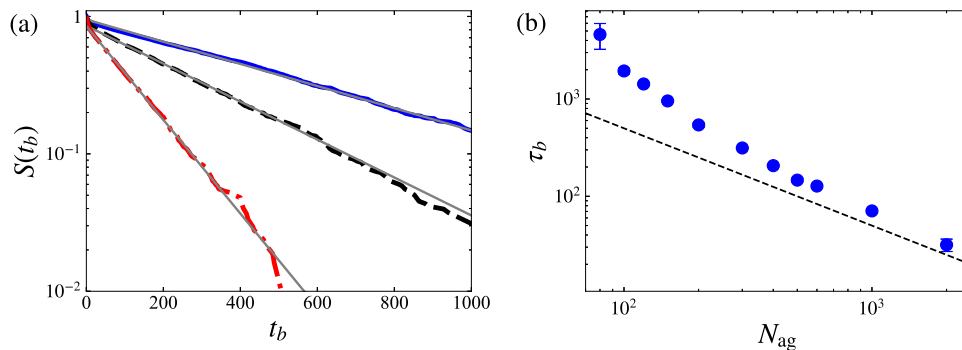


FIG. 4. (a) Survival function $S(t_b)$ of micelles for $N_{ag} = 200$ (blue solid line), 300 (black dashed line), and 600 (red dotted-dashed line) at equilibrium with $k_B T = 1$. Gray lines are exponential fits to the data. (b) Average lifetime τ_b of micelles as a function of the aggregation number N_{ag} with $k_B T = 1$. The black dashed line indicates $\tau_b \propto N_{ag}^{-1}$. The error bars in (b) denote the standard deviations for three independent simulations.

an exponential decay. In Fig. 4(b), we show τ_b as a function of N_{ag} . Figure 4(b) shows $\tau_b \propto N_{ag}^{-1}$ for $N_{ag} \gtrsim 300$. This scaling is consistent with the model proposed by Cates,²³ which assumes that scission of chains occurs with a constant probability per unit time per unit length.

We have seen that τ_r is a monotonically increasing function of N_{ag} [Fig. 3(b)], whereas τ_b is a monotonically decreasing function of N_{ag} [Fig. 4(b)]. In Fig. 5(a), we show τ_r and τ_b as functions of N_{ag} with $k_B T = 1$. These two timescales τ_r and τ_b cross each other at a certain aggregation number N_Λ and we define τ_Λ as $\tau_r(N_\Lambda)$. Since $\tau_b(N_{ag}) < \tau_r(N_{ag})$ for $N_{ag} > N_\Lambda$ [Fig. 5(a)], the rotational relaxation of micelles with $N_{ag} \gtrsim N_\Lambda$ proceeds with the aid of scission. Here, note that τ_r corresponds to the rotational relaxation time of micelles without scission kinetics. In order to evaluate their longest relaxation time τ including the effect of scission kinetics, we extend the theory for the Rouse chain with the scission and recombination processes²⁴ to unentangled micelles. In contrast to the original theory, we do not assume that relaxation modes obey the Rouse theory. Instead, we use numerical results of τ_r and τ_b [Fig. 5(a)]. We then expect τ to follow

$$\tau(N_{ag}) = \begin{cases} \tau_r(N_{ag}) & (N_{ag} \lesssim N_\Lambda), \\ \tau_\Lambda & (N_{ag} \gtrsim N_\Lambda). \end{cases} \quad (19)$$

For $N_{ag} \lesssim N_\Lambda$, since τ_b is larger than τ_r , the rotational relaxation of micelles is not affected by their scission, leading to $\tau(N_{ag}) = \tau_r(N_{ag})$. In contrast, for $N_{ag} \gtrsim N_\Lambda$, micelles can break into small micelles in a shorter time than $\tau_r(N_{ag})$. As a result, their rotational relaxation proceeds through that of these small micelles

with a shorter relaxation time than $\tau_r(N_{ag})$. Similarly, the generated small micelles are likely to break into even smaller micelles before their rotational relaxation if $\tau_b < \tau_r$. Consequently, micelles such that $\tau_r \simeq \tau_b$ (i.e., $N_{ag} \simeq N_\Lambda$) determine the longest relaxation time. Therefore, micelles with $N_{ag} \gtrsim N_\Lambda$ relax with a characteristic time of the order of τ_Λ for which τ_r is comparable to τ_b [Fig. 5(a)]. This means that the slower relaxation timescales ($\tau_r > \tau_\Lambda$) disappear due to the rapid scission of large micelles with $N_{ag} \gtrsim N_\Lambda$. In other words, N_Λ defines the largest segment that behaves in a similar way to polymer chains (i.e., chains without scission kinetics). This is why micelles with $N_{ag} \gtrsim N_\Lambda$ have a common longest relaxation time irrespective of N_{ag} . We show τ_Λ as a function of $1/k_B T$ in Fig. 5(b) and confirm the Arrhenius dependence. In addition, the inset in Fig. 5(b) shows that N_Λ is also a monotonically increasing function of $1/k_B T$. To the best of our knowledge, this is the first evaluation of the longest relaxation time of unentangled surfactant micelles from the rotational relaxation time τ_r and the average lifetime τ_b using molecular simulations.

To confirm the validity of τ_Λ obtained by our extended method of Faivre and Gardissat,²⁴ we first examine the mean squared displacement (MSD) ($\langle \Delta r^2 \rangle$) of surfactant molecules. Regarding polymer chains, the MSD of monomers is known to exhibit a subdiffusive regime when $t \lesssim \tau$ and a normal regime when $t \gtrsim \tau$ in DPD simulations,⁴⁴ where τ is the longest relaxation time of polymer chains. Huang *et al.*²¹ reported that linear chains with a kinetic model for scission and recombination showed a similar crossover from subdiffusion to normal diffusion around τ_Λ obtained with the original method of Faivre and Gardissat.²⁴ We show the compensated MSD $\langle \Delta r^2 \rangle / t$ of surfactant molecules for various $k_B T$ as a function of t/τ_Λ

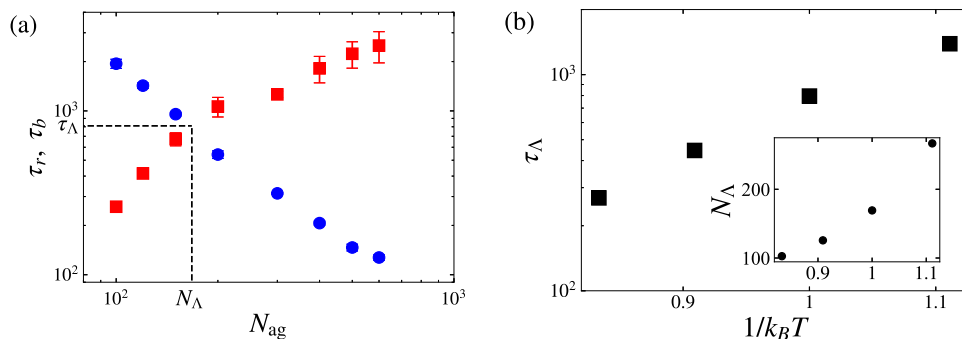


FIG. 5. (a) Rotational relaxation time τ_r (red square) and average lifetime τ_b (blue circle) as functions of the aggregation number N_{ag} with $k_B T = 1$. Their intersection defines the longest relaxation time τ_Λ of micelles for $N_{ag} \gtrsim N_\Lambda$. The error bars denote the standard deviations for three independent simulations. (b) Longest relaxation time τ_Λ as a function of $1/k_B T$. The inset shows N_Λ as a function of $1/k_B T$.

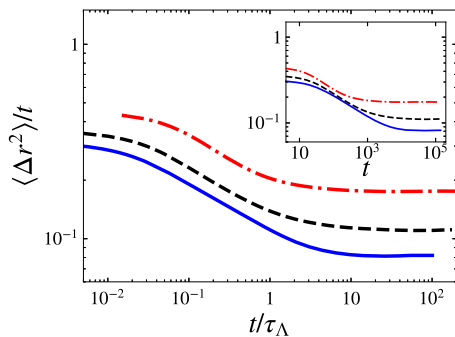


FIG. 6. Compensated MSD $\langle \Delta r^2 \rangle / t$ of surfactant molecules as a function of the normalized time t / τ_Λ with $k_B T = 0.9$ (blue solid line), $k_B T = 1$ (black dashed line), and $k_B T = 1.2$ (red dotted-dashed line). The inset shows $\langle \Delta r^2 \rangle / t$ as a function of t .

in Fig. 6. For $0.1 \lesssim t / \tau_\Lambda \lesssim 1$, $\langle \Delta r^2 \rangle / t$ has a negative slope, indicating the subdiffusion of surfactant molecules. In contrast, for $t / \tau_\Lambda \gtrsim 10$, $\langle \Delta r^2 \rangle / t$ is flat, indicating the normal diffusion. Thus, we confirm that $\langle \Delta r^2 \rangle$ shows a gradual crossover from subdiffusion to normal diffusion around $t / \tau_\Lambda = O(1)$, which is consistent with the property of the MSD in other systems mentioned above. For comparison, we show $\langle \Delta r^2 \rangle / t$ as a function of t in the inset of Fig. 6. It is then more evident that τ_Λ serves as an appropriate timescale. However, $\langle \Delta r^2 \rangle$ includes the contribution from all the surfactant molecules, which belong to micelles of different sizes. We need to conduct a more detailed analysis of the MSD to directly prove the relevance of τ_Λ , which is beyond the scope of the present study.

To summarize this section, we evaluated the longest relaxation time τ_Λ of unentangled surfactant micelles from the rotational relaxation time τ_r and the average lifetime τ_b of micelles at equilibrium by extending the concept proposed by Faivre and Gardissat.²⁴ We confirmed that the longest relaxation time serves as the relevant timescale at equilibrium by investigating the MSD. In Sec. III B, we

focus on micelles with $N_{\text{ag}} \gtrsim N_\Lambda$ and verify the relevance of τ_Λ under shear flow by using conditional statistics based on N_{ag} .

B. Flow-induced scission

In this section, we investigate the flow-induced scission of wormlike micelles under shear flow. We demonstrate that flow-induced scission occurs when the Weissenberg number $Wi_\Lambda = \tau_\Lambda \dot{\gamma}$ is larger than a threshold value.

To reveal the effect of flow-induced scission, we investigate the statistical properties of the micellar lifetime under shear flow. We show in Fig. 7(a) the survival function $S(t_b)$ of micelles for $N_{\text{ag}} = 300$ with $k_B T = 1$ for different Wi_Λ . For $Wi_\Lambda = 4.0$, $S(t_b)$ hardly differs from $S(t_b)$ at equilibrium ($Wi_\Lambda = 0$), whereas for $Wi_\Lambda = 8.0$ and 16 , $S(t_b)$ declines with Wi_Λ . This indicates that, in addition to scission through thermal fluctuations, flow-induced scission occurs more significantly as Wi_Λ increases. Figure 7(b) shows the N_{ag} dependence of τ_b for the same Wi_Λ as in Fig. 7(a). As shown in Fig. 7(a), for $Wi_\Lambda = 4.0$, the shear flow does not affect τ_b for any N_{ag} considered here. In contrast, for $Wi_\Lambda = 8.0$ and 16 , the shear flow reduces τ_b more significantly as Wi_Λ increases. Note that N_{ag} dependence of τ_b remains unchanged under shear flow for all Wi_Λ considered here. In other words, the shear flow affects τ_b of micelles such that $N_{\text{ag}} \gtrsim N_\Lambda$ with a factor independent of N_{ag} . Figure 7(b) implies that the threshold value of Wi_Λ for the decrease in τ_b is also independent of N_{ag} . Therefore, it is reasonable to conclude that micelles with $N_{\text{ag}} \gtrsim N_\Lambda$ have a common longest relaxation time, as explained in Eq. (19), and, consequently, their scission is promoted to the same degree by the shear flow.

Next, we demonstrate that τ_Λ defined as the value for which $\tau_r(N_{\text{ag}}) = \tau_b(N_{\text{ag}})$ [Fig. 5(a)] serves as the characteristic timescale in flow-induced scission. For this purpose, we consider several systems where τ_Λ takes different values by conducting DPD simulations with different $k_B T$ [Fig. 5(b)]. We show τ_b for $N_{\text{ag}} = 300, 400$, and 500 as a function of Wi_Λ in Fig. 8. Here, τ_b is normalized by the value τ_b^0 at equilibrium for a given N_{ag} . For comparison, we show τ_b / τ_b^0 as a function of $\dot{\gamma}$ in the inset of Fig. 8. The increase in

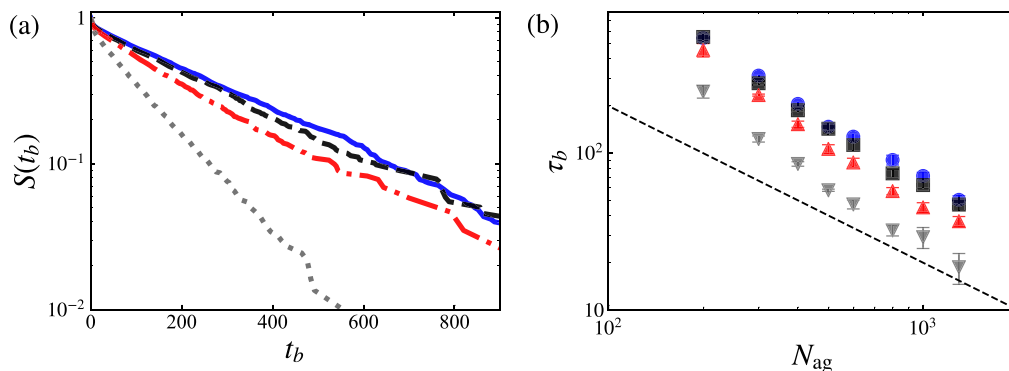


FIG. 7. (a) Survival function $S(t_b)$ of micelles with $N_{\text{ag}} = 300$ for $Wi_\Lambda = 0$ (blue solid line), 4.0 (black dashed line), 8.0 (red dotted-dashed line), and 16 (gray dotted line) with $k_B T = 1$. (b) Average lifetime τ_b of micelles as a function of the aggregation number N_{ag} for $Wi_\Lambda = 0$ (blue circle), 4.0 (black square), 8.0 (red triangle), and 16 (gray inverted triangle) with $k_B T = 1$. The black dashed line in (b) indicates $\tau_b \propto N_{\text{ag}}^{-1}$. The error bars in (b) denote the standard deviations for three independent simulations.

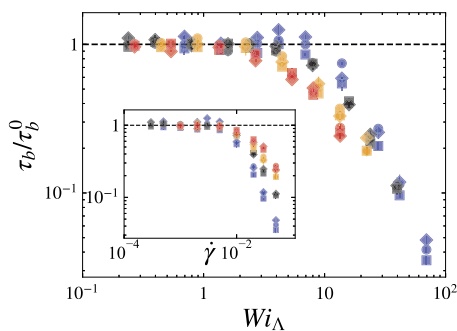


FIG. 8. Average lifetime τ_b normalized by the value τ_b^0 at equilibrium as a function of the Weissenberg number Wi_Λ for $N_{ag} = 300$ (\circ), 400 (\square), and 500 (\diamond) with $k_B T = 0.9$ (blue), 1 (black), 1.1 (orange), and 1.2 (red). The inset shows τ_b/τ_b^0 as a function of the shear rate $\dot{\gamma}$. The black dashed line indicates $\tau_b/\tau_b^0 = 1$. The error bars denote the standard deviations for three independent simulations.

τ_b/τ_b^0 with $k_B T$ for fixed $\dot{\gamma}$ indicates that scission of micelles is promoted more as the temperature is decreased for given $\dot{\gamma}$. In other words, the $\dot{\gamma}$ dependence of τ_b/τ_b^0 significantly differs depending on $k_B T$; micelles at a lower temperature are more likely to be broken by the shear flow. We emphasize that we can take into account this $k_B T$ dependence by using τ_Λ . More concretely, all the data for different $k_B T$ as well as for different N_{ag} follow a single function of Wi_Λ (Fig. 8). The reason for this collapse is that micelles with $N_{ag} \gtrsim N_\Lambda$ are aligned and elongated by the shear flow with a timescale τ_Λ , as we will discuss below (see Fig. 9). We have also confirmed that if $\phi \lesssim 0.1$, τ_b/τ_b^0 follows the same function shown in Fig. 8. Since ϕ does not significantly change the properties of micelles within the dilute regime, it is reasonable that τ_b/τ_b^0 is independent of ϕ ($\lesssim 0.1$). Interestingly, as shown in Fig. 8, $\tau_b \simeq \tau_b^0$ when Wi_Λ is smaller than a threshold value Wi_c ($\simeq 4$), indicating that flow-induced scission does not occur, whereas τ_b monotonically decreases with Wi_Λ for $Wi_\Lambda > Wi_c$. However, it is difficult to discuss this

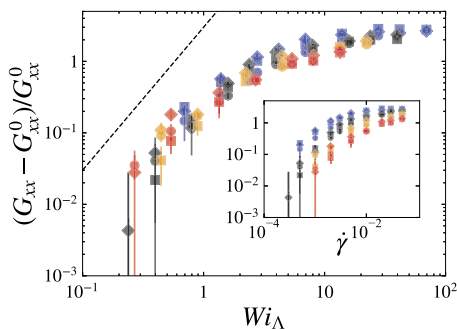


FIG. 9. Relative change $(G_{xx} - G_{xx}^0)/G_{xx}^0$ of diagonal component G_{xx} of the gyration tensor normalized by the value G_{xx}^0 at equilibrium as a function of the Weissenberg number Wi_Λ for $N_{ag} = 300$ (\circ), 400 (\square), and 500 (\diamond) with $k_B T = 0.9$ (blue), 1 (black), 1.1 (orange), and 1.2 (red). The black dashed line indicates $(G_{xx} - G_{xx}^0)/G_{xx}^0 \propto Wi_\Lambda^2$. The inset shows $(G_{xx} - G_{xx}^0)/G_{xx}^0$ as a function of the shear rate $\dot{\gamma}$. The error bars denote the standard deviations for three independent simulations.

threshold Weissenberg number Wi_c in more detail due to the limited accuracy of τ_b . We examine Wi_c in another way, as described below (see Fig. 11). Since τ_r monotonically increases with N_{ag} [Fig. 3(b)], it may be counterintuitive that the threshold shear rate for flow-induced scission is independent of N_{ag} for fixed $k_B T$. As mentioned in Sec. III A, since the considered micelles satisfy $\tau_b(N_{ag}) < \tau_r(N_{ag})$ (i.e., $N_{ag} > N_\Lambda$), the slower relaxation timescales ($\tau_r > \tau_\Lambda$) disappear as a result of scission faster than the rotational relaxation, thus leading to a common threshold shear rate. In other words, the segment of size N_Λ determines the effects of shear flow on micelles with $N_{ag} \gtrsim N_\Lambda$.

We investigate the gyration tensor defined by Eq. (17), which characterizes the micellar structure, to demonstrate that τ_Λ plays a vital role in the orientation and elongation of micelles under shear flow. Figure 9 shows the relative change $(G_{xx} - G_{xx}^0)/G_{xx}^0$ of the diagonal component G_{xx} corresponding to the flow direction, where G_{xx}^0 is the value at equilibrium for fixed N_{ag} . All the data for different $k_B T$ and N_{ag} approximately collapse on a single function of Wi_Λ , which indicates that Wi_Λ determines the orientation and elongation of micelles under shear flow. This is consistent with the previous study,²⁵ which used linear chain models including scission and recombination kinetics. Therefore, we conclude that Wi_Λ determines the effects of the shear flow on micelles, such as orientation and elongation, thus determining the degree of flow-induced scission, i.e., τ_b/τ_b^0 , because the elongation of micelles causes their scission.^{19,45} For comparison, we show $(G_{xx} - G_{xx}^0)/G_{xx}^0$ as a function of $\dot{\gamma}$ in the inset of Fig. 9. Without considering τ_Λ , $(G_{xx} - G_{xx}^0)/G_{xx}^0$ depends on $\dot{\gamma}$ differently for each $k_B T$; its $\dot{\gamma}$ dependence varies greatly depending on $k_B T$. Therefore, τ_Λ is an important property for understanding the shear-rate dependence of the micellar dynamics under shear flow. In addition, $(G_{xx} - G_{xx}^0)/G_{xx}^0$ is independent of N_{ag} for fixed $k_B T$ and $\dot{\gamma}$. This is consistent with our claim that micelles with $N_{ag} \gtrsim N_\Lambda$ have a common longest relaxation time for given $k_B T$. In Fig. 9, we find that $(G_{xx} - G_{xx}^0)/G_{xx}^0 \propto Wi_\Lambda^2$ holds for $Wi_\Lambda \lesssim 1$, which is a well-known characteristic of polymers.⁴⁶ This indicates that micelles behave similarly to polymers under shear flow for moderate Wi_Λ .

Here, note that τ_b/τ_b^0 and $(G_{xx} - G_{xx}^0)/G_{xx}^0$ do not completely follow a single curve, as shown in Figs. 8 and 9, indicating that there exist other relevant factors. For example, regarding semiflexible polymers, stiffness significantly affects their properties under shear flow.⁴⁷ In addition, although we do not consider the effect of branched micellar structures, these complex structures may also play a role in the micellar dynamics as demonstrated in a previous study.⁴⁸ Thus, topological characterization of micelles using the recently developed method⁴⁹ can provide valuable information about the detailed mechanism of flow-induced scission. This is an important near-future study.

We have seen that our analysis of the lifetime using conditional statistics clearly reveals how flow-induced scission affects individual micelles. Next, to examine how flow-induced scission affects the distribution of N_{ag} , we focus on the Wi_Λ dependence of the probability density function $P(N_{ag})$ of N_{ag} . Figure 10 shows $P(N_{ag})$ for several values of Wi_Λ with $k_B T = 1$. For $Wi_\Lambda < Wi_c$ ($\simeq 4$), $P(N_{ag})$ is independent of Wi_Λ . This indicates that flow-induced scission does not occur for $Wi_\Lambda < Wi_c$, which is consistent with the results shown in Fig. 8. For Wi_Λ larger than Wi_c , in contrast, $P(N_{ag})$ for large N_{ag} decreases and the distribution shifts to

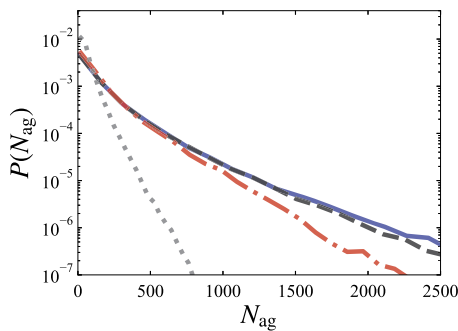


FIG. 10. Probability density function $P(N_{\text{ag}})$ of the aggregation number N_{ag} for $Wi_{\Lambda} = 0$ (blue solid line), 4.0 (black dashed line), 8.0 (red dotted-dashed line), and 40 (gray dotted line) with $k_B T = 1$.

smaller N_{ag} as Wi_{Λ} increases. Therefore, it is clear that when Wi_{Λ} exceeds Wi_c , flow-induced scission occurs, and then the population of large micelles declines. Note that for $Wi_{\Lambda} = 0$, $P(N_{\text{ag}})$ cannot be expressed by a single exponential function, whereas the model proposed by Cates²³ predicts the exponential distribution of micellar length. As shown in Fig. 4(b), micelles with $N_{\text{ag}} \lesssim 300$ do not satisfy the assumption that chains can break with a fixed probability per unit length per unit time. Therefore, it is reasonable that $P(N_{\text{ag}})$ does not obey a single exponential function, although we focus on N_{ag} instead of micellar length. Dhakal and Sureshkumar⁵⁰ also reported that $P(N_{\text{ag}})$ did not obey an exponential function for charged micelles when the salt-to-surfactant concentration ratio was smaller than 1.

Before closing this article, we focus on the average number \bar{N}_{mic} of micelles in the system and the mean aggregation number \bar{N}_{ag} , which reflect the onset of flow-induced scission, as discussed below. Figure 11(a) shows \bar{N}_{mic} normalized by the value \bar{N}_{mic}^0 at equilibrium as a function of Wi_{Λ} . We find that $\bar{N}_{\text{mic}}/\bar{N}_{\text{mic}}^0$ is expressed by a single function of Wi_{Λ} irrespective of $k_B T$. In addition, Fig. 11(a) provides clear evidence that flow-induced scission occurs for $Wi_{\Lambda} > Wi_c$

(≈ 4). These observations are also valid for \bar{N}_{ag} shown in Fig. 11(b). These results support the conclusion that τ_{Λ} is a relevant timescale of unentangled surfactant micelles. In the case of the parameters used in the present study, the average properties of the system, such as \bar{N}_{mic} and \bar{N}_{ag} , are also determined by Wi_{Λ} . Since more than 65% of surfactants in the system belong to micelles with $N_{\text{ag}} \gtrsim N_{\Lambda}$ at equilibrium with $k_B T = 1$, it is quite reasonable that τ_{Λ} has a dominant influence on the average properties. Therefore, if we conduct experiments on the surfactant solutions where most surfactant molecules belong to micelles with $N_{\text{ag}} \gtrsim N_{\Lambda}$, the longest relaxation time τ_{Λ} will be a relevant timescale of the system. In other words, the experimentally obtained bulk properties such as viscosity are likely to be characterized by τ_{Λ} . Indeed, as shown in Appendix B, Wi_{Λ} determines the rheological properties of the considered solutions. Note that we take full advantage of molecular simulations to evaluate the longest relaxation time. We propose a method to obtain τ_{Λ} through the N_{ag} dependences of τ_r and τ_b , which are usually unavailable in experiments.

IV. CONCLUSIONS

In the present study, we have investigated flow-induced scission of wormlike micelles in nonionic surfactant solutions under shear flow with DPD. Although flow-induced scission may be intuitively obvious, a quantitative understanding of this phenomenon has been unsatisfactory. This was mainly due to the difficulty of obtaining a large amount of micellar scission data for various aggregation numbers N_{ag} and the lack of methods to estimate the relevant timescale of individual unentangled micelles. With the aid of the DPD method, which allows us to simulate large systems for long timescales, we can obtain a sufficient amount of data to discuss the statistical properties of micellar scission in detail.

In order to elucidate flow-induced scission in terms of micellar timescales, we have proposed a method to estimate the longest relaxation time τ_{Λ} of unentangled surfactant micelles from the rotational relaxation time τ_r (Fig. 3) and the average lifetime τ_b (Fig. 4) at equilibrium in the absence of shear flow. Using the concept proposed by Faivre and Gardissat,²⁴ which originally assumed the Rouse

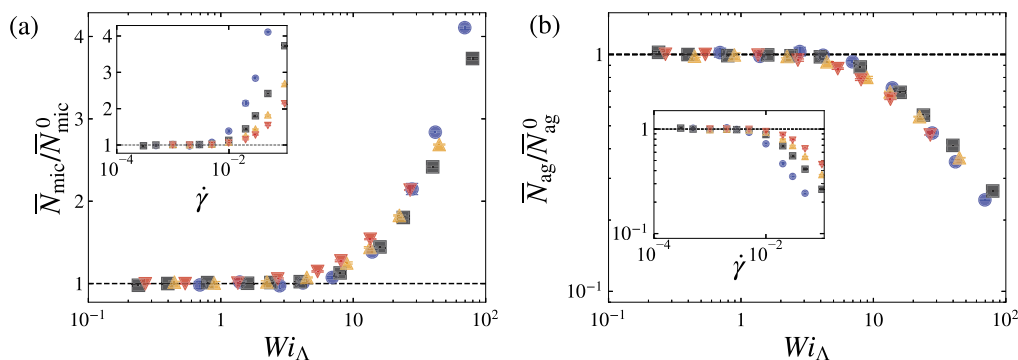


FIG. 11. (a) Average number \bar{N}_{mic} of micelles in the system normalized by the value \bar{N}_{mic}^0 at equilibrium as a function of the Weissenberg number Wi_{Λ} . The black dashed line indicates $\bar{N}_{\text{mic}}/\bar{N}_{\text{mic}}^0 = 1$. The inset shows $\bar{N}_{\text{mic}}/\bar{N}_{\text{mic}}^0$ as a function of the shear rate $\dot{\gamma}$. (b) Mean aggregation number \bar{N}_{ag} normalized by the value \bar{N}_{ag}^0 at equilibrium as a function of Wi_{Λ} . The black dashed line indicates $\bar{N}_{\text{ag}}/\bar{N}_{\text{ag}}^0 = 1$. The inset shows $\bar{N}_{\text{ag}}/\bar{N}_{\text{ag}}^0$ as a function of $\dot{\gamma}$. Different symbols correspond to different values of $k_B T$: blue circle, 0.9; black square, 1; orange triangle, 1.1; red inverted triangle, 1.2.

chain with scission and recombination processes, we have evaluated τ_Λ from the intersection of $\tau_r(N_{\text{ag}})$ and $\tau_b(N_{\text{ag}})$ [Fig. 5(a)]. This concept means that relaxation modes such that $\tau_r \gtrsim \tau_\Lambda$ disappear because the timescale of micellar scission is shorter than that of rotational relaxation for these modes. In fact, as shown in Fig. 6, the MSD of surfactant molecules has provided evidence that τ_Λ is a crucial timescale at equilibrium. More concretely, τ_Λ is comparable to the crossover time from subdiffusion to normal diffusion for different temperatures. These results are in agreement with the previous study using linear chains with a kinetic model for scission and recombination.²⁵ Thus, we have found that the concept proposed by Faivre and Gardissat²⁴ is also applicable to unentangled surfactant micelles when we develop the method to evaluate the longest relaxation time using data from molecular simulations.

One of the most important conclusions of the present study is that τ_Λ is a crucial timescale for flow-induced scission of wormlike surfactant micelles under shear flow. Our analysis relies on conditional statistics based on the aggregation number N_{ag} , which reveals the shear flow effect on individual micelles in detail. Indeed, the survival function $S(t_b)$ of micelles for fixed N_{ag} has demonstrated that flow-induced scission occurs for high shear rates [Fig. 7(a)]. We have also found in Fig. 7(b) that for large N_{ag} , $\tau_b \propto N_{\text{ag}}^{-1}$ holds even under shear flow, similarly to the equilibrium state [Fig. 4(b)]. To demonstrate the role of τ_Λ in the shear-rate dependence of τ_b , we have conducted DPD simulations for different temperatures. We have shown that the Weissenberg number Wi_Λ , which is defined as the product of the longest relaxation time τ_Λ and the shear rate $\dot{\gamma}$, determines τ_b under shear flow (Fig. 8). To the best of our knowledge, this is the first attempt to show that τ_b can be characterized by the nondimensionalized shear rate. Since Wi_Λ also determines the diagonal component G_{xx} of the gyration tensor G_{ij} (Fig. 9), the Wi_Λ dependence of τ_b is associated with the elongation of micelles. However, since the collapse is slightly unclear in Figs. 8 and 9, our numerical results suggest that, in addition to Wi_Λ , there exist other important factors, such as stiffness and branched micellar structures. We have examined the Wi_Λ dependence of the micellar distribution (Fig. 10), the average number of micelles [Fig. 11(a)], and the average aggregation number [Fig. 11(b)]. We then conclude that flow-induced micellar scission occurs when Wi_Λ is larger than a threshold Weissenberg number Wi_c . Although $Wi_c \simeq 4$ in the examined system, we speculate that Wi_c depends on various factors, such as the conservative force coefficients a_{ij} in the DPD method.

In the present study, we have revealed the shear-rate dependence of flow-induced scission focusing on nonionic surfactants. However, further studies are required. First, our results are restricted to the case of nonionic surfactant micelles. Regarding the scission of ionic surfactant micelles, we must consider the effect of counterions.¹⁹ However, the proposed method to evaluate τ_Λ from τ_r and τ_b is applicable to molecular simulations of unentangled surfactant micelles regardless of the kind of surfactant. Thus, it is an interesting future study to investigate flow-induced scission of different kinds of surfactant micelles and reveal their differences, which will provide helpful insight into the practical applications of surfactant solutions. Second, we have not revealed the physical mechanism behind the statistical properties of flow-induced scission. To overcome this deficiency, it is necessary to reveal the

dynamics of individual micelles, such as alignment and elongation.¹⁹ Flow-induced scission is expected to have a great impact on micellar dynamics, thus leading to complicated behavior different from that of polymer chains (i.e., chains without scission kinetics). In addition, it is essential to understand flow-induced scission in terms of mechanics such as stress and energy.^{18,19} Third, we should take into account the structural diversity in micelles. Here, we focused on conditional statistics based on aggregation numbers. However, as shown in Appendix A, micelles can form different structures even for a given aggregation number. It is, therefore, important to conduct a more detailed conditional analysis considering micellar structures.

ACKNOWLEDGMENTS

The authors are grateful to Professor T. Inoue, Professor T. Kawakatsu, and Professor N. Matubayasi for valuable remarks on the first version of the manuscript. The present study was supported, in part, by the JSPS Grants-in-Aid for Scientific Research (Grant Nos. 20H02068 and 21J21061). The DPD simulations were mainly conducted under the auspices of the NIFS Collaboration Research Programs (Grant No. NIFS20KNSS145). A part of the simulations was conducted using the JAXA Supercomputer System Generation 3 (JSS3).

AUTHOR DECLARATIONS

Conflict of Interest

The authors have no conflicts to disclose.

Author Contributions

Yusuke Koide: Conceptualization (equal); Data curation (lead); Formal analysis (lead); Investigation (lead); Methodology (equal); Validation (lead); Visualization (lead); Writing – original draft (lead); Writing – review & editing (equal). **Susumu Goto:** Conceptualization (equal); Funding acquisition (lead); Project administration (lead); Resources (lead); Supervision (lead); Writing – original draft (supporting); Writing – review & editing (equal).

DATA AVAILABILITY

The data that support the findings of this study are available from the corresponding author upon reasonable request.

APPENDIX A: STRUCTURAL PROPERTIES OF MICELLES AT EQUILIBRIUM

We adopt conditional statistics based on the aggregation number N_{ag} . In this appendix, we show the relationship between the micellar structure and N_{ag} .

First, we show snapshots of micelles for various N_{ag} in Fig. 12, which qualitatively demonstrate how micelles grow with N_{ag} . Surfactants form spherical, rodlike, wormlike, and branched wormlike micelles as N_{ag} increases. Note, however, that micelles can form various structures even for a given N_{ag} . In particular, for $N_{\text{ag}} \gtrsim 200$, both linear and branched micelles exist.

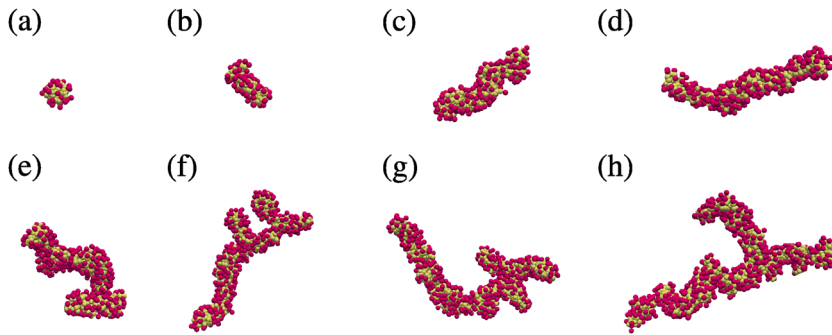


FIG. 12. Snapshots of micelles for (a) $N_{ag} = 40$, (b) 70, (c) 200, (d) 300, (e) 400, (f) 500, (g) 600, and (h) 700.

Next, to quantitatively investigate the structures of micelles, we focus on the gyration radius R_g and relative shape anisotropy⁵¹ K^2 . These quantities are expressed as

$$R_g^2 = G_{xx} + G_{yy} + G_{zz} \quad (\text{A1})$$

and

$$K^2 = 1 - 3 \frac{G_{xx}G_{yy} + G_{yy}G_{zz} + G_{zz}G_{xx} - G_{xy}^2 - G_{yz}^2 - G_{zx}^2}{(G_{xx} + G_{yy} + G_{zz})^2} \quad (\text{A2})$$

in terms of the gyration tensor G_{ij} defined by Eq. (17). The relative shape anisotropy K^2 can take values between 0 and 1. A spherical structure is characterized by $K^2 \approx 0$, and a rodlike structure is characterized by $K^2 \approx 1$. Figure 13 shows R_g and K^2 as functions of N_{ag} . Figure 13(a) shows that $R_g \propto N_{ag}^{1/3}$ for $N_{ag} \lesssim 50$. This behavior changes around $N_{ag} = 50$. Since $R_g \propto N_{ag}^{1/3}$ holds for spherical micelles,³¹ the structural transition of micelles occurs around $N_{ag} = 50$. In addition, Fig. 13(b) demonstrates that $K^2 \approx 0$ for $N_{ag} \lesssim 50$, and K^2 becomes much larger for $N_{ag} \gtrsim 50$. Therefore, micelles are spherical for $N_{ag} \lesssim 50$, whereas micelles are rodlike for $N_{ag} \gtrsim 50$. Note also a gradual decrease of K^2 for $N_{ag} \gtrsim 200$ [Fig. 13(b)]. This is because micelles for $N_{ag} \gtrsim 200$ are wormlike and flexible. These quantitative results are consistent with the visualizations of micellar structures shown in Fig. 12. Thus, R_g and K^2 enable us to estimate the structure of micelles (i.e., spherical, rodlike, or wormlike). According to these criteria for micellar structures in terms of N_{ag} , we mainly deal with rodlike and wormlike micelles in the present study. We need to conduct a more detailed analysis to

characterize branched structures. This is an important near-future study.

APPENDIX B: RHEOLOGICAL PROPERTIES OF SURFACTANT SOLUTIONS

In this appendix, we show the rheological properties of the considered surfactant solutions. The stress tensor σ can be calculated using the Irving–Kirkwood equation,⁵²

$$\sigma = -\frac{1}{V} \left\langle \sum_{i=1}^N m \mathbf{v}_i \mathbf{v}_i + \sum_{i=1}^N \sum_{j>i}^N \mathbf{r}_{ij} \mathbf{F}_{ij} \right\rangle, \quad (\text{B1})$$

where V is the volume of the system. Then, the viscosity η and the first normal stress coefficient Ψ_1 are evaluated by

$$\eta = \frac{\sigma_{yx}}{\dot{\gamma}} \quad \text{and} \quad \Psi_1 = \frac{\sigma_{xx} - \sigma_{yy}}{\dot{\gamma}^2}, \quad (\text{B2})$$

respectively. Figure 14 shows the Wi_Λ dependences of η and Ψ_1 for several $k_B T$. Here, η is shown in the form of $(\eta - \eta_s)/(\eta_0 - \eta_s)$, where η_s is the viscosity of water at a given $k_B T$ and η_0 is the viscosity of the solution at the lowest shear rate. The value of Ψ_1 is normalized by $\Psi_{1,0}$ at the lowest shear rate. Both η and Ψ_1 decrease with Wi_Λ when $Wi_\Lambda \gtrsim 1$. One might think that flow-induced scission causes this shear thinning. However, since the alignment of micelles in the flow direction also contributes to the shear thinning, a more detailed analysis is required to identify the effect of flow-induced scission on rheological properties. As shown in Fig. 14(b), the first normal stress

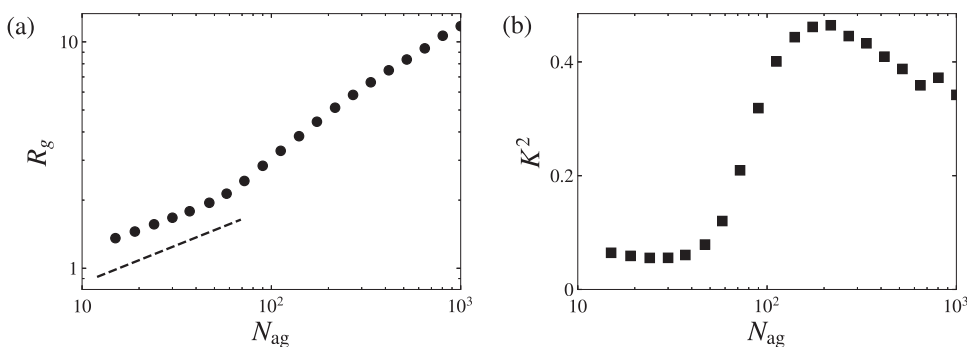


FIG. 13. (a) Gyration radius R_g and (b) relative shape anisotropy K^2 as functions of the aggregation number N_{ag} with $k_B T = 1$. The dashed line in (a) indicates $R_g \propto N_{ag}^{1/3}$.

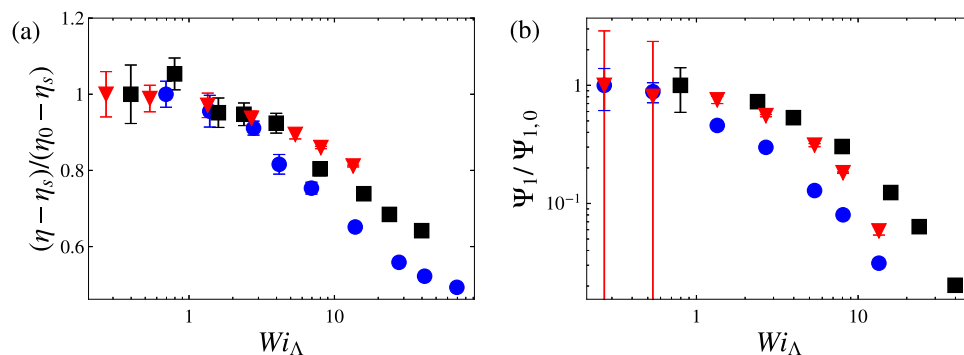


FIG. 14. (a) Increase in viscosity $\eta - \eta_s$ of the solutions from the solvent viscosity η_s normalized by the value $\eta_0 - \eta_s$ at the lowest shear rate and (b) first normal stress coefficient Ψ_1 normalized by the value $\Psi_{1,0}$ at the lowest shear rate as functions of the Weissenberg number Wi_Λ . Different symbols correspond to different values of $k_B T$: blue circle, 0.9; black square, 1; red inverted triangle, 1.2. The error bars denote the standard deviations for three independent simulations.

difference is positive, indicating that the surfactant solutions have viscoelasticity.

REFERENCES

- T. Shikata, H. Hirata, and T. Kotaka, "Micelle formation of detergent molecules in aqueous media: Viscoelastic properties of aqueous cetyltrimethylammonium bromide solutions," *Langmuir* **3**, 1081 (1987).
- Z. Chu, C. A. Dreiss, and Y. Feng, "Smart wormlike micelles," *Chem. Soc. Rev.* **42**, 7174 (2013).
- M. D. Warholic, G. M. Schmidt, and T. J. Hanratty, "The influence of a drag-reducing surfactant on a turbulent velocity field," *J. Fluid Mech.* **388**, 1 (1999).
- M. J. Lawrence, "Surfactant systems: Their use in drug delivery," *Chem. Soc. Rev.* **23**, 417 (1994).
- R. K. Prud'homme and G. G. Warr, "Elongational flow of solutions of rodlike micelles," *Langmuir* **10**, 3419 (1994).
- C.-M. Chen and G. G. Warr, "Light scattering from wormlike micelles in an elongational field," *Langmuir* **13**, 1374 (1997).
- J. P. Rothstein, "Transient extensional rheology of wormlike micelle solutions," *J. Rheol.* **47**, 1227 (2003).
- S. Chen and J. P. Rothstein, "Flow of a wormlike micelle solution past a falling sphere," *J. Non-Newtonian Fluid Mech.* **116**, 205 (2004).
- A. Kalb, L. A. Villasmil U., and M. Cromer, "Role of chain scission in cross-slot flow of wormlike micellar solutions," *Phys. Rev. Fluids* **2**, 071301 (2017).
- M. B. Khan and C. Sasmal, "Effect of chain scission on flow characteristics of wormlike micellar solutions past a confined microfluidic cylinder: A numerical analysis," *Soft Matter* **16**, 5261 (2020).
- P. A. Vasquez, G. H. McKinley, and L. P. Cook, "A network scission model for wormlike micellar solutions. I. Model formulation and viscometric flow predictions," *J. Non-Newtonian Fluid Mech.* **144**, 122 (2007).
- S. Dutta and M. D. Graham, "Mechanistic constitutive model for wormlike micelle solutions with flow-induced structure formation," *J. Non-Newtonian Fluid Mech.* **251**, 97 (2018).
- R. J. Hommel and M. D. Graham, "Constitutive modeling of dilute wormlike micelle solutions: Shear-induced structure and transient dynamics," *J. Non-Newtonian Fluid Mech.* **295**, 104606 (2021).
- S. J. Candau, F. Merikhi, G. Waton, and P. Lemaréchal, "Temperature-jump study of elongated micelles of cetyltrimethylammonium bromide," *J. Phys. France* **51**, 977 (1990).
- F. Kern, P. Lemaréchal, S. J. Candau, and M. E. Cates, "Rheological properties of semidilute and concentrated aqueous solutions of cetyltrimethylammonium bromide in the presence of potassium bromide," *Langmuir* **8**, 437 (1992).
- I. Couillet, T. Hughes, G. Maitland, F. Candau, and S. J. Candau, "Growth and scission energy of wormlike micelles formed by a cationic surfactant with long unsaturated tails," *Langmuir* **20**, 9541 (2004).
- F. Liu, D. Liu, W. Zhou, F. Chen, and J. Wei, "Coarse-grained molecular dynamics simulations of the breakage and recombination behaviors of surfactant micelles," *Ind. Eng. Chem. Res.* **57**, 9018 (2018).
- T. Mandal and R. G. Larson, "Stretch and breakage of wormlike micelles under uniaxial strain: A simulation study and comparison with experimental results," *Langmuir* **34**, 12600 (2018).
- A. Sambasivam, A. V. Sangwai, and R. Sureshkumar, "Dynamics and scission of rodlike cationic surfactant micelles in shear flow," *Phys. Rev. Lett.* **114**, 158302 (2015).
- M. Kröger and R. Makhloufi, "Wormlike micelles under shear flow: A microscopic model studied by nonequilibrium-molecular-dynamics computer simulations," *Phys. Rev. E* **53**, 2531 (1996).
- C.-C. Huang, H. Xu, and J.-P. Ryckaert, "Kinetics and dynamic properties of equilibrium polymers," *J. Chem. Phys.* **125**, 094901 (2006).
- J. T. Padding, E. S. Boek, and W. J. Briels, "Dynamics and rheology of wormlike micelles emerging from particulate computer simulations," *J. Chem. Phys.* **129**, 074903 (2008).
- M. E. Cates, "Reptation of living polymers: Dynamics of entangled polymers in the presence of reversible chain-scission reactions," *Macromolecules* **20**, 2289 (1987).
- G. Faivre and J. L. Gardissat, "Viscoelastic properties and molecular structure of amorphous selenium," *Macromolecules* **19**, 1988–1996 (1986).
- C.-C. Huang, J.-P. Ryckaert, and H. Xu, "Structure and dynamics of cylindrical micelles at equilibrium and under shear flow," *Phys. Rev. E* **79**, 041501 (2009).
- P. J. Hoogerbrugge and J. M. V. A. Koelman, "Simulating microscopic hydrodynamic phenomena with dissipative particle dynamics," *Europhys. Lett.* **19**, 155 (1992).
- P. Español and P. Warren, "Statistical mechanics of dissipative particle dynamics," *Europhys. Lett.* **30**, 191 (1995).
- S. Yamamoto and S. Hyodo, "Mesoscopic simulation of the crossing dynamics at an entanglement point of surfactant threadlike micelles," *J. Chem. Phys.* **122**, 204907 (2005).
- N. Arai, K. Yasuoka, and Y. Masubuchi, "Spontaneous self-assembly process for threadlike micelles," *J. Chem. Phys.* **126**, 244905 (2007).
- S. Meng, J. Zhang, Y. Wang, X. Li, C. Wu, T. Hou, L. Xiao, and G. Lu, "Simulating the rheology of surfactant solution using dissipative particle dynamics," *Mol. Simul.* **41**, 772 (2015).
- R. L. Anderson, D. J. Bray, A. Del Regno, M. A. Seaton, A. S. Ferrante, and P. B. Warren, "Micelle formation in alkyl sulfate surfactants using dissipative particle dynamics," *J. Chem. Theory Comput.* **14**, 2633 (2018).
- H. Wang, X. Tang, D. M. Eike, R. G. Larson, and P. H. Koenig, "Scission free energies for wormlike surfactant micelles: Development of a simulation protocol, application, and validation for personal care formulations," *Langmuir* **34**, 1564 (2018).
- C. R. Wand, M. Panoukidou, A. Del Regno, R. L. Anderson, and P. Carbone, "The relationship between wormlike micelle scission free energy and micellar composition: The case of sodium lauryl ether sulfate and cocamidopropyl betaine," *Langmuir* **36**, 12288 (2020).

- ³⁴Y. Kobayashi, H. Gomyo, and N. Arai, "Molecular insight into the possible mechanism of drag reduction of surfactant aqueous solution in pipe flow," *Int. J. Mol. Sci.* **22**, 7573 (2021).
- ³⁵R. D. Groot and P. B. Warren, "Dissipative particle dynamics: Bridging the gap between atomistic and mesoscopic simulation," *J. Chem. Phys.* **107**, 4423 (1997).
- ³⁶J. Li, J. Wang, Q. Yao, Y. Zhang, Y. Yan, and J. Zhang, "The biphasic effect of ABA triblock copolymers on the self-assembly of surfactants: Insight from dissipative particle dynamics," *Mol. Syst. Des. Eng.* **4**, 921 (2019).
- ³⁷M.-T. Lee, R. Mao, A. Vishnyakov, and A. V. Neimark, "Parametrization of chain molecules in dissipative particle dynamics," *J. Phys. Chem. B* **120**, 4980 (2016).
- ³⁸R. L. Anderson, D. J. Bray, A. S. Ferrante, M. G. Noro, I. P. Stott, and P. B. Warren, "Dissipative particle dynamics: Systematic parametrization using water-octanol partition coefficients," *J. Chem. Phys.* **147**, 094503 (2017).
- ³⁹E. Lavagnini, J. L. Cook, P. B. Warren, M. J. Williamson, and C. A. Hunter, "A surface site interaction point method for dissipative particle dynamics parametrization: Application to alkyl ethoxylate surfactant self-assembly," *J. Phys. Chem. B* **124**, 5047 (2020).
- ⁴⁰A. W. Lees and S. F. Edwards, "The computer study of transport processes under extreme conditions," *J. Phys. C: Solid State Phys.* **5**, 1921 (1972).
- ⁴¹D. J. Evans and G. Morriss, *Statistical Mechanics of Nonequilibrium Liquids* (Cambridge University Press, 2008).
- ⁴²A. Vishnyakov, M.-T. Lee, and A. V. Neimark, "Prediction of the critical micelle concentration of nonionic surfactants by dissipative particle dynamics simulations," *J. Phys. Chem. Lett.* **4**, 797 (2013).
- ⁴³E. L. Kaplan and P. Meier, "Nonparametric estimation from incomplete observations," *J. Am. Stat. Assoc.* **53**, 457 (1958).
- ⁴⁴W. Jiang, J. Huang, Y. Wang, and M. Laradji, "Hydrodynamic interaction in polymer solutions simulated with dissipative particle dynamics," *J. Chem. Phys.* **126**, 044901 (2007).
- ⁴⁵J. Gao, S. Li, X. Zhang, and W. Wang, "Computer simulations of micelle fission," *Phys. Chem. Chem. Phys.* **12**, 3219 (2010).
- ⁴⁶C.-C. Huang, R. G. Winkler, G. Sutmann, and G. Gompper, "Semidilute polymer solutions at equilibrium and under shear flow," *Macromolecules* **43**, 10107 (2010).
- ⁴⁷R. G. Winkler, "Conformational and rheological properties of semiflexible polymers in shear flow," *J. Chem. Phys.* **133**, 164905 (2010).
- ⁴⁸S. Dhakal and R. Sureshkumar, "Anomalous diffusion and stress relaxation in surfactant micelles," *Phys. Rev. E* **96**, 012605 (2017).
- ⁴⁹B. O. Conchuir, K. Gardner, K. E. Jordan, D. J. Bray, R. L. Anderson, M. A. Johnston, W. C. Swope, A. Harrison, D. R. Sheehy, and T. J. Peters, "Efficient algorithm for the topological characterization of worm-like and branched micelle structures from simulations," *J. Chem. Theory Comput.* **16**, 4588 (2020).
- ⁵⁰S. Dhakal and R. Sureshkumar, "Topology, length scales, and energetics of surfactant micelles," *J. Chem. Phys.* **143**, 024905 (2015).
- ⁵¹D. N. Theodorou and U. W. Suter, "Shape of unperturbed linear polymers: Polypropylene," *Macromolecules* **18**, 1206 (1985).
- ⁵²J. H. Irving and J. G. Kirkwood, "The statistical mechanical theory of transport processes. IV. The equations of hydrodynamics," *J. Chem. Phys.* **18**, 817 (1950).